

SCIENTIFIC REPORTS



OPEN

Multiple aspects of male germ cell development and interactions with Sertoli cells require inositol hexakisphosphate kinase-1

Chenglai Fu^{1,2}, Tomas Rojas², Alfred C. Chin², Weiwei Cheng³, Isaac A. Bernstein², Lauren K. Albacarys², William W. Wright⁴ & Solomon H. Snyder^{2,5,6}

Inositol hexakisphosphate kinase-1 (IP6K1) is required for male fertility, but the underlying mechanisms have been elusive. Here, we report that IP6K1 is required for multiple aspects of male germ cell development. This development requires selective interactions between germ cells and Sertoli cells, namely apical ectoplasmic specialization. Spermiation (sperm release) requires tubulobulbar complexes. We found that the apical ectoplasmic specialization and tubulobulbar complexes were poorly formed or disrupted in *IP6K1* KO mice. Deletion of *IP6K1* elicited several aberrations, including: 1, sloughing off of round germ cells; 2, disorientation and malformation of elongating/elongated spermatids; 3, degeneration of acrosomes; 4, defects in germ-Sertoli cell interactions and 5, failure of spermiation. Eventually the sperm cells were not released but phagocytosed by Sertoli cells leading to an absence of sperm in the epididymis.

Inositol hexakisphosphate kinase (IP6K) comprises a family of three kinases, namely IP6K1, IP6K2 and IP6K3^{1–3}. Functions of IP6Ks have been inferred from studies of mice with targeted deletion of IP6K1, IP6K2 and IP6K3. IP6K1 is involved in diverse functions. It determines insulin release⁴, regulates cell migration^{5,6}, histone demethylation⁷ and cell metabolisms^{8–10}. Important for this study, it was reported that *IP6K1* KO male mice are infertile with no sperm in the epididymides^{1,11}. Recently, Bhandari and associates reported that IP6K1 is essential for the formation of the chromatoid body¹¹. They found that the chromatoid body is absent in *IP6K1* KO round spermatids, and the mutant spermatids failed to complete differentiation¹¹. However, despite these advances, the influence of IP6K1 upon male germ cell development has not been fully delineated.

Spermatogenesis, the generation of motile sperm cells from spermatogonial stem cells, is largely regulated by follicle stimulating hormone (FSH) and luteinizing hormone (LH) released from the pituitary gland as well as testosterone produced by Leydig cells. The microenvironment of the seminiferous epithelium also is critical for sperm development¹². In seminiferous tubules, germ cells are surrounded by Sertoli cells, which orchestrate the organization of testicular structures. Sertoli cells are “nurse” cells that influence the survival, replication, differentiation, and movement of germ cells via direct contact and by controlling the environment milieu within the seminiferous tubules¹³. Sertoli cells provide physical and nutritional support for germ cells^{14,15} as well as secreting factors to control maintenance and self-renewal of spermatogonial stem cells¹⁶. Sertoli cells protect germ cells by forming the blood-testis barrier and expressing immunoregulatory factors, thereby creating a local tolerogenic environment optimal for survival of nonsequestered auto-antigenic germ cells¹⁷. Sertoli cells also function as phagocytes to eliminate degenerated cells^{18,19}.

¹Department of Physiology and Pathophysiology, Tianjin Medical University, Tianjin, 300070, China. ²The Solomon H. Snyder Department of Neuroscience, Johns Hopkins University School of Medicine, Baltimore, MD, 21205, USA. ³Division of Neuropathology, Department of Pathology, Johns Hopkins University School of Medicine, Baltimore, MD, 21205, USA. ⁴Department of Biochemistry and Molecular Biology, Johns Hopkins Bloomberg School of Public Health, Baltimore, MD, 21205, USA. ⁵Department of Pharmacology and Molecular Sciences, Johns Hopkins University School of Medicine, Baltimore, MD, 21205, USA. ⁶Department of Psychiatry and Behavioral Sciences, Johns Hopkins University School of Medicine, Baltimore, MD, 21205, USA. Correspondence and requests for materials should be addressed to C.F. (email: cfu9@jhmi.edu) or S.H.S. (email: ssnyder@jhmi.edu)

In mice, spermatogenesis has been classified into 12 stages according to the arrangement of different germ cells that are developmentally synchronized in the seminiferous epithelium. In addition, the differentiation of round spermatids into mature, motile spermatozoa is divided into 16 steps. At step 16 mature, motile sperm are released (spermiation) corresponding to stage VII to VIII in spermatogenesis²⁰.

Developing round and elongating/elongated spermatids must maintain stable attachments with Sertoli cells to prevent sloughing of immature germ cells from the seminiferous epithelium, which may result in infertility²¹. The apical ectoplasmic specialization (ES) is a unique adhesion junction formed between elongating/elongated spermatids and Sertoli cells, and is crucial for attachment of spermatids as well as their movement and orientation during spermatogenesis²². Disruption of germ cell-Sertoli cell interactions²³ or spermatid polarization²⁴ leads to spermatogenic defects and infertility. The molecular composition of apical ES includes integral membrane proteins, adaptor proteins, signaling proteins and cytoskeletal proteins. However, little is known about the regulation of apical ES dynamics^{22,25}.

The apical tubulobulbar complex (TBC) is another linkage between maturing spermatids and Sertoli cells, formed by cytoplasmic processes extending from spermatids into the neighboring Sertoli cells²⁶. In mice apical TBCs are transiently formed at spermatogenic stage VII prior to sperm release and function to remove excess cytoplasm from spermatids²⁷ and to remove adhesion junctions between spermatids and Sertoli cells^{26,28}. The apical TBC is comprised of a long proximal tubule followed by a bulb, then a short distal tubule and a coated pit²⁶. Actin filaments are highly enriched in apical TBCs²⁹. Defects of apical TBCs caused by chemical treatment or genetic mutation result in spermiation failure^{30–32}.

In the present study we explored the roles of IP6K1 in male germ cell development. The elongating/elongated spermatids of *IP6K1* KO were disoriented and malformed. The acrosomes of *IP6K1* KO spermatids were also degenerated during differentiation. Defective apical ES and malformed apical TBCs were apparent in the *IP6K1* mutants. Eventually, the defective sperm cells failed to release and were engulfed by Sertoli cells at stage VII and stage VIII in the seminiferous epithelium of KO mice, which can account for the sperm deficits.

Results

Deletion of IP6K1 leads to male infertility caused by scarce and malformed sperms. Deletion of *IP6K1* in mice was shown to elicit male infertility^{1,11}. In agreement with this finding, we observed a complete absence of offspring from *IP6K1* deleted males, whereas fertility appeared normal in *IP6K1* KO females (Fig. S1a). In contrast to the lack of fertility of *IP6K1* KO males, mice with deletion of *IP6K2*, *IP6K3* or double knockout of *IP6K2* and *IP6K3* displayed normal fertility (Fig. 1a). We also examined the sexual behavior and ability of mice to mate, which appeared to be normal in the *IP6K1* KO males (Fig. 1b).

Reproductive behavior and spermatogenesis is regulated by levels of reproductive hormones. However, plasma levels of FSH, LH and testosterone were normal in *IP6K1* KO male mice (Fig. S1b–d). Thus, the fertility defect of *IP6K1* KO male mice does not arise from hormonal deregulation.

We collected motile sperm cells from epididymides and observed very little cellular content and no motile sperm cells in the *IP6K1* KO mice (Fig. 1c). We observed severed sperm tails in the *IP6K1* KO preparations with some residual DNA surrounded by sperm tails (Figs 1d and S1e).

Deletion of IP6K1 causes sloughing of round germ cells. We first looked at the gross morphology of the reproductive organs. Testes of the *IP6K1* KOs were reduced in size (Fig. S2a,b), and testicular weight was diminished by about 20 percent (Fig. S2b). We then looked at the microscopic morphology. In testes of *IP6K1* KOs, spermatids were more loosely attached to Sertoli cells than for wild-type animals (Fig. 2a), and round spermatids were dislodged (Fig. 2b). The sloughing of germ cells in *IP6K1* KO seminiferous tubules was confirmed by the presence of round cells in the cauda epididymides of *IP6K1* mutant mice (Fig. 2c). Thus, deletion of *IP6K1* affected interactions between germ cells and Sertoli cells.

We examined sperm in testes by staining sperm tails for acetyl- α -tubulin, which revealed a virtually total loss of mature sperms in *IP6K1* KOs (Fig. 2d). In both caput and cauda epididymides of wild type animals, the lumens were typically filled with sperm cells. The lumens of *IP6K1* KO epididymides, however, were devoid of sperm, whereas levels in *IP6K2* and *IP6K3* KOs were comparable to wild-type animals (Fig. S2c,d).

IP6K1 deletion causes malformation of elongating/elongated spermatids. We examined the different stages of spermatogenesis in testes (Fig. 3). In *IP6K1* KOs, elongating/elongated spermatids displayed aberrant morphology. The steps 12–16 elongating/elongated spermatids of *IP6K1* mutants appeared disoriented and irregularly shaped (Fig. 3a–f). By contrast, no obvious defect was seen in steps 1–8 round spermatids in *IP6K1* KOs (Fig. S3).

Immunofluorescence staining of testes revealed abundant IP6K1 localized to the germ cells of wild-type mice, which was completely absent in *IP6K1* KOs (Fig. S4a). We noted major differences in the cellular localizations of IP6K1, IP6K2 and IP6K3 in testes (Fig. S4b). IP6K1 was ubiquitously expressed in germ cells; IP6K2 occurred in primary spermatocytes, while the expression of IP6K3 was low and only evident in step 12 spermatids (Fig. S4b). IP6K1 was expressed in elongating/elongated spermatids (Fig. S4c,d), implying that structural/functional defects in these cells in mutant mice stems from the loss of IP6K1 (Fig. 3). We explored a potential loss of Sertoli and Leydig cells in the *IP6K1* KOs. Staining of Sertoli cells for GATA4 and of Leydig cells with calretinin revealed relatively normal numbers of these cell types (Fig. S5a,b).

IP6K1 deletion causes disorientation of spermatids and failure of spermiation. We examined cellular morphology in the testes by Toluidine blue staining (Fig. 4). Disorientation, defined as a deviation of more than 90 degree from pointing to basement membrane perpendicular³³, and abnormal morphology of elongating/elongated spermatids were pronounced in the mutants (Fig. 4a–c). Dislodged round spermatids were

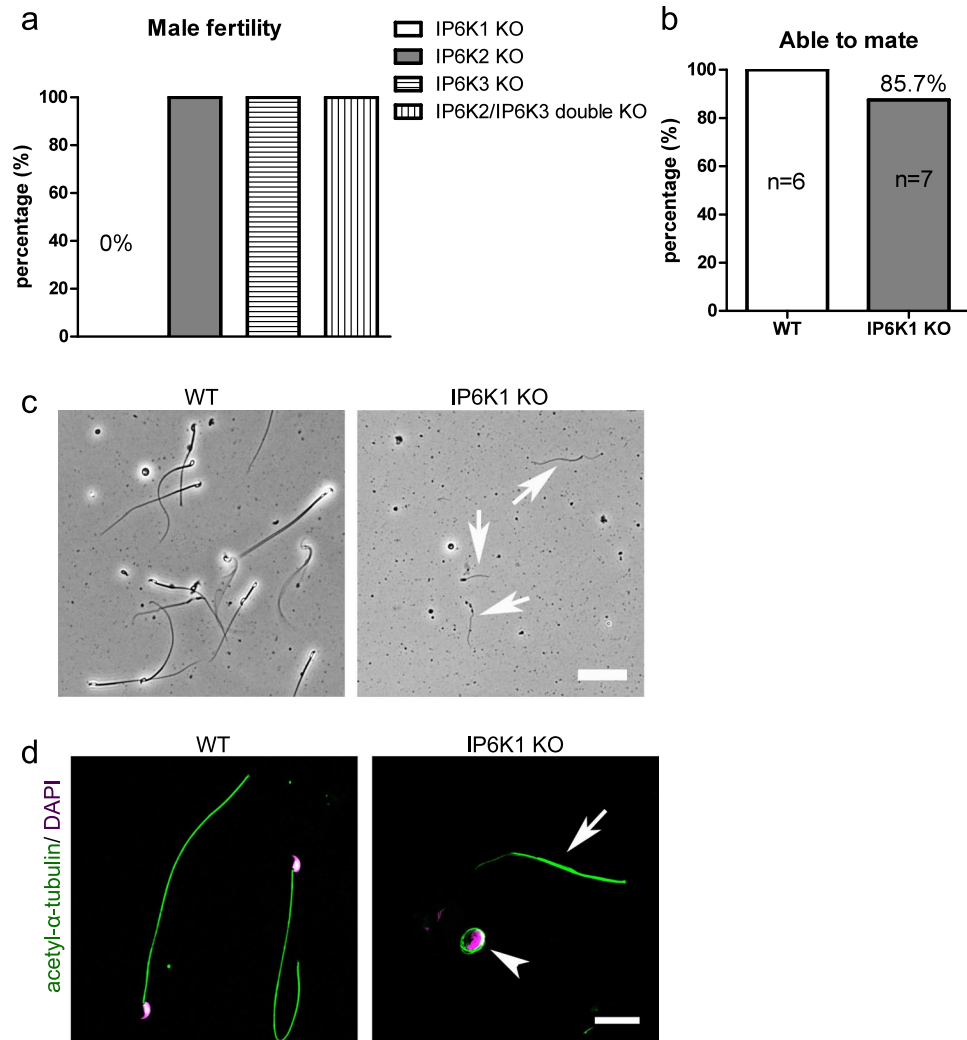


Figure 1. Infertility in *IP6K1* deleted males was caused by scarce and malformed sperm. **(a)** None of *IP6K1* KO male mice ($n = 7$) impregnate wild type females. By contrast, *IP6K2* KO males ($n = 6$), *IP6K3* KO males ($n = 6$) and *IP6K2/IP6K3* double KO males ($n = 6$) are able to produce progeny. **(b)** *IP6K1* KO male mice ($n = 7$) were set to mate with wild type female mice, mating plugs were found in six of seven wild type female mice. Six pairs of WT male and female mice were set as controls. **(c,d)** Sperm cells were isolated from epididymides. **(c)** Bright-field microscopy shows severed sperm tails (arrows) but no motile sperm cells in *IP6K1* KOs. Scale bar 50 μm . **(d)** Immunostaining of acetyl- α -tubulin for sperm tails. Nuclei were stained by DAPI. Severed sperm tails (arrow) and sperm heads coiled by sperm tails (arrowhead) were seen in the *IP6K1* mutants. Scale bar 20 μm .

evident in the lumens of seminiferous tubules of *IP6K1* KOs (Fig. 4b,c and e). Most striking was the substantial engulfment of sperm by Sertoli cells (Fig. 4d–f). In wild type mice, the sperm were released at stage VII–VIII, and the lumens were full of sperm (Fig. 4d). However, sperm were not released in *IP6K1* KOs. Instead, they were “eaten” by Sertoli cells (Fig. 4d–f). The phagocytosis of sperm cells was prominent at stage VII (Fig. 4d) and stage VIII (Fig. 4e), when they should be released. The engulfed sperm cells were also observed at stage IX (Fig. 4f).

To further assess mechanisms underlying the abnormalities in *IP6K1* KOs, we evaluated different steps of spermatid differentiation by electron microscopy (Fig. 5). Development of round spermatids was relatively normal in *IP6K1* KOs (Fig. 5a–f). The most notable abnormalities occurred in the disposition of elongating/elongated spermatids at steps 9–16 (Fig. 5g–l). Disorientation and malformation of spermatids was marked at steps 9–16 (Fig. 5g–l), indicating that spermatids lose cell polarity in *IP6K1* KOs. At steps 12–16 in the KOs (Fig. 5j–l), the structure of spermatid heads was abnormal or improperly formed. The step 16 spermatids were not released but eventually engulfed by Sertoli cells in *IP6K1* KO stage VII and VIII seminiferous tubules (Fig. 6a). Severed sperm tails were seen in stage IX of the seminiferous epithelium of *IP6K1* KOs (Fig. 6b).

IP6K1 deletion disrupts cell polarity and causes malformation of acrosome. We examined cell polarity of the spermatids. In *IP6K1* KO seminiferous tubules, the elongating spermatids lost orientation (Fig. 6c), and some elongating spermatids showed double acrosome granules (Fig. 6d), indicating that cell polarity was disrupted. We examined the structure of elongating/elongated spermatids in *IP6K1* KOs and found malformations

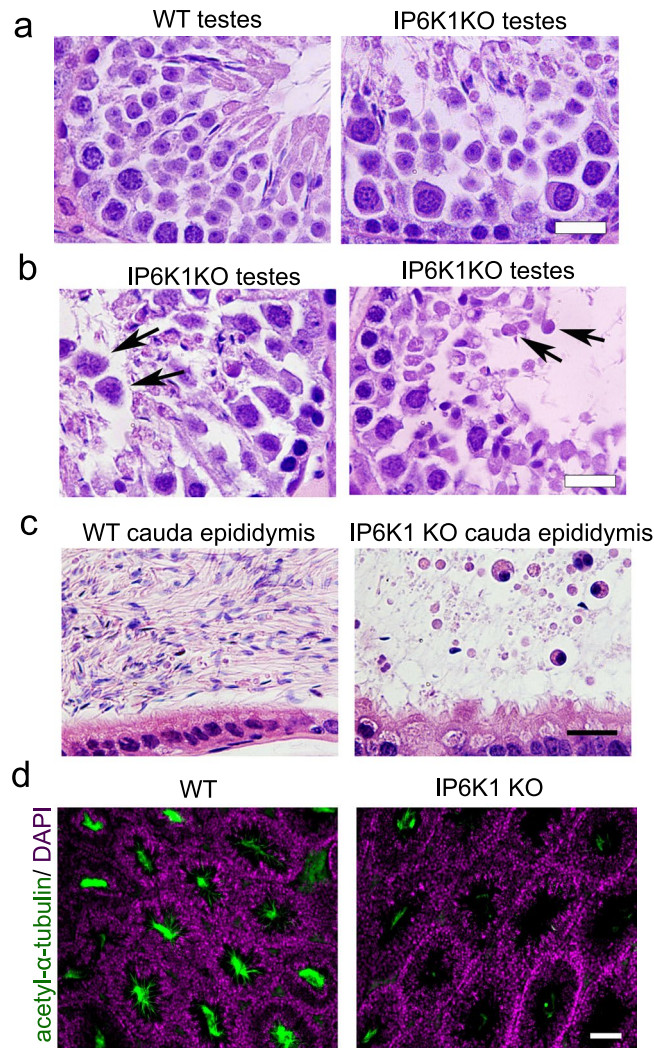


Figure 2. Deletion of IP6K1 elicited sloughing of round germ cells. **(a,b)** H&E staining of testes **(a)** Germ cells in *IP6K1* KO seminiferous tubules are more loosely connected to Sertoli cells. Scale bar 20 μ m. **(b)** Round germ cells were sloughed off and appeared in the lumina of seminiferous tubules (arrows). Scale bar 20 μ m. **(c)** H&E staining of cauda epididymides. Round germ cells were seen in *IP6K1* KO cauda epididymides. scale bar 20 μ m. **(d)** Immunostaining of sperm tails in testes with anti acetyl- α -tubulin antibody; DAPI stains nucleus. Scale bar 100 μ m.

of acrosomes (Fig. 6e–g). Disconnected acrosomes were first seen in step 12 spermatids (Fig. 6e). The integrity of the acrosomes gradually degenerated during differentiation in *IP6K1* KOs (Fig. 6f,g).

IP6K1 deletion disrupts apical ectoplasmic specialization. We examined the interaction between elongating/elongated spermatids and Sertoli cells, known as the apical ectoplasmic specialization (ES) (Fig. 7a–e). The actin filament bundles that align perpendicular to the Sertoli cell plasma membrane were a characteristic feature of the apical ES in the WT preparations (Fig. 7a–e). At step 8 of spermatid differentiation, the spermatid nuclei made contact with the cell surface. The apical ES was formed between the spermatids and Sertoli cells of WT mice. In *IP6K1* KOs, however, no characteristic apical ES was observed at step 8 (Fig. 7a). Apical ES was observable in step 10–16 spermatids of the *IP6K1* KOs. However, the structures were disrupted. The apical ES was not well formed in step 10–12 spermatids (Fig. 7b,c), appeared to be collapsing in step 14 spermatids of *IP6K1* KOs (Fig. 7d), and collapsed in step 16 spermatids of the *IP6K1* mutants (Fig. 7e).

The staining of F-actin on testes showed that in WT seminiferous tubules, sperm cells covered with abundant actin filaments. In *IP6K1* KOs, however, the cells were only partially associated with actin bundles (Fig. 7f,g).

IP6K1 deletion disrupts apical tubulobulbar complexes. Sperm release requires normal functioning of apical tubulobulbar complexes^{30–32}. We examined the morphology of apical tubulobulbar complexes (TBCs) in the *IP6K1* mutants (Fig. 8a). The apical TBCs in the *IP6K1* KOs were malformed with absence of proximal tubules and swelling of the bulbs (Fig. 8a). Thus, the defective apical TBCs lead to spermiation failure (Fig. 4d,e) and excess residual cytoplasm in *IP6K1* KO spermatids (Fig. 8b)^{27,32}.

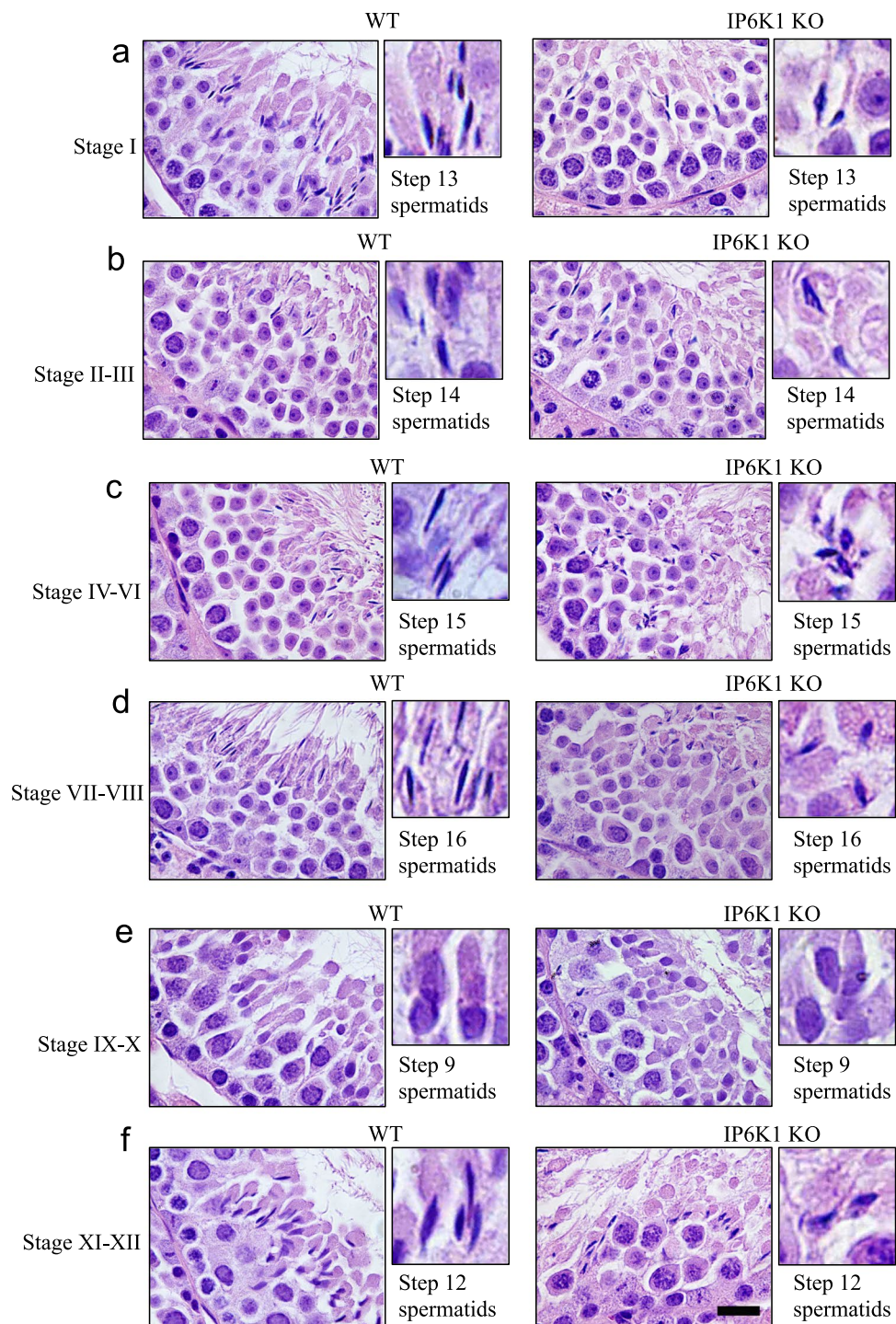


Figure 3. Deletion of IP6K1 elicited disorientation and malformation of elongating/elongated spermatids. (a–f) H&E staining of WT and *IP6K1* KO testes. Stages of seminiferous tubules were determined by spermatid developmental status. (a,b,c,d,f) Cell polarity and morphology of the step 12–16 elongating/elongated spermatids were disrupted in *IP6K1* KOs (insets). Scale bar 20 μ m.

Discussion

In the present study we have developed insights into the role of IP6K1 in male germ cell development. The infertility of *IP6K1* KO mice is evidently caused by deficits in both quantity and quality of sperm. We observed several defects: 1, sloughing of round germ cells; 2, disorientation and malformation of elongating/elongated spermatids; 3, degeneration of acrosomes; 4, disrupted apical ES and apical TBCs; 5, failure of spermiation in the *IP6K1* KO mice. Eventually sperm were phagocytosed by Sertoli cells, a mechanism which may fully account for the observed sperm deficit^{23,24}.

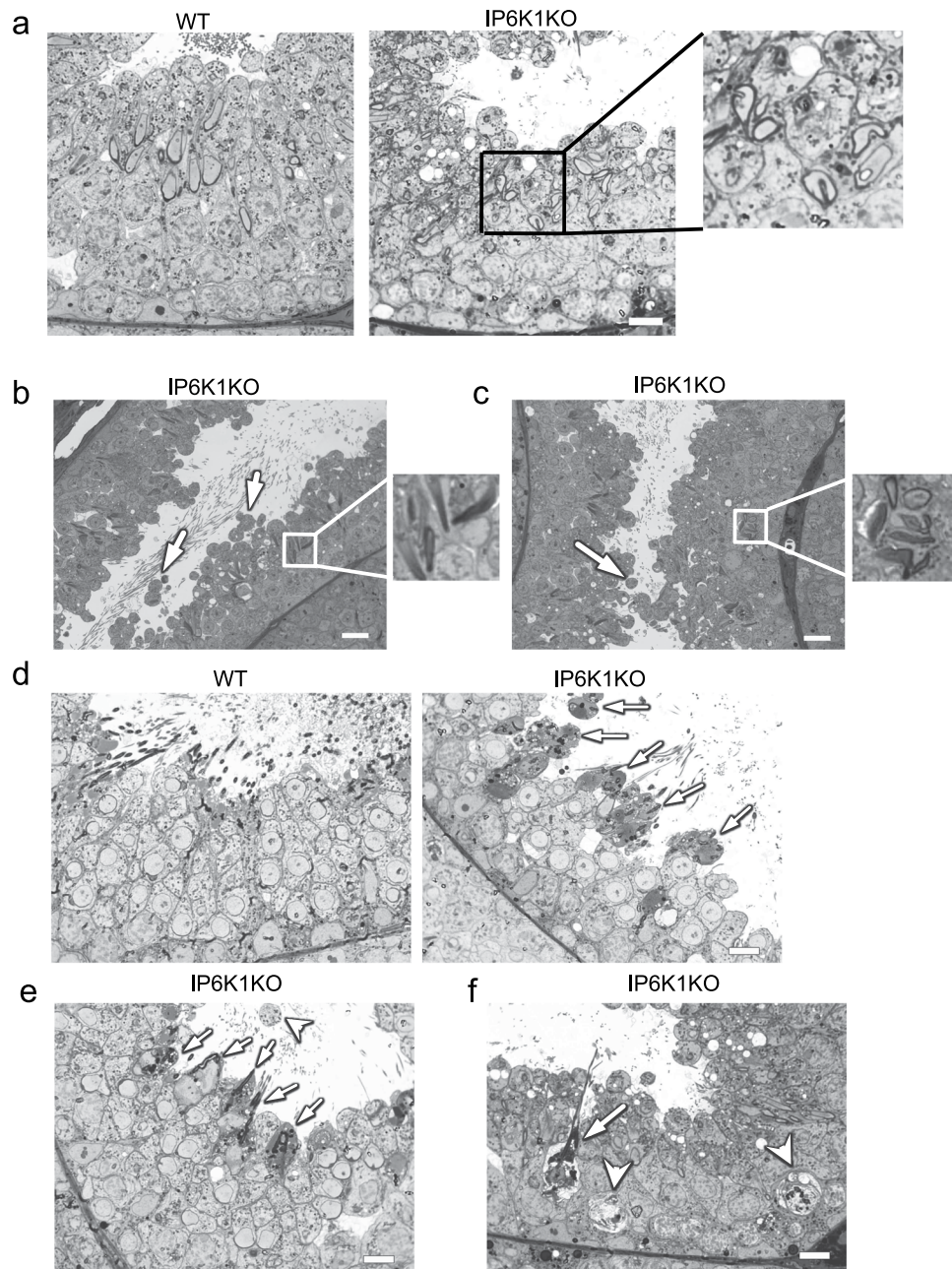


Figure 4. Spermiogenesis failure and phagocytosis of sperm by Sertoli cells in *IP6K1* KOs. (a–f) Toluidine blue staining of testes. (a) In stage X seminiferous tubules of *IP6K1* KOs, the elongating spermatids were disoriented (inset). Scale bar 10 μm . (b) In stage I seminiferous tubules of *IP6K1* mutants, the elongated spermatids were disoriented (inset) and some round spermatids were sloughed off (arrows). Scale bar 20 μm . (c) In stage II–III seminiferous tubules of *IP6K1* KOs, the elongated spermatids were disoriented and malformed (inset), some round spermatids were dislodged (arrow). Scale bar 20 μm . (d) In stage VII seminiferous tubules. Sperm cells were not released but engulfed by Sertoli cells in *IP6K1* KOs (arrows). Scale bar 10 μm . (e) In stage VIII seminiferous tubules of *IP6K1* KOs, sperm cells were “eaten” by Sertoli cells (arrows). Sloughed off round spermatids were evident in the lumens (arrowhead). Scale bar 10 μm . (f) In stage IX seminiferous tubules of *IP6K1* mutants, “choking down” sperms killed Sertoli cells (arrow). Arrowheads point to phagosomes (digested spermatocytes) within Sertoli cells. Scale bar 10 μm .

Our results are consistent with previous reports^{1,11}, including: the expression of *IP6K1* in germ cells; complete loss of fertility in *IP6K1* KO males but normal fertility in females; normal testosterone levels in *IP6K1* KO males; reduced size and weight of testes in *IP6K1* KO mice; absence of mature spermatozoa, and premature release of round cells in *IP6K1* KO epididymides; abnormal morphology and incomplete nuclear condensation in elongating/elongated spermatids.

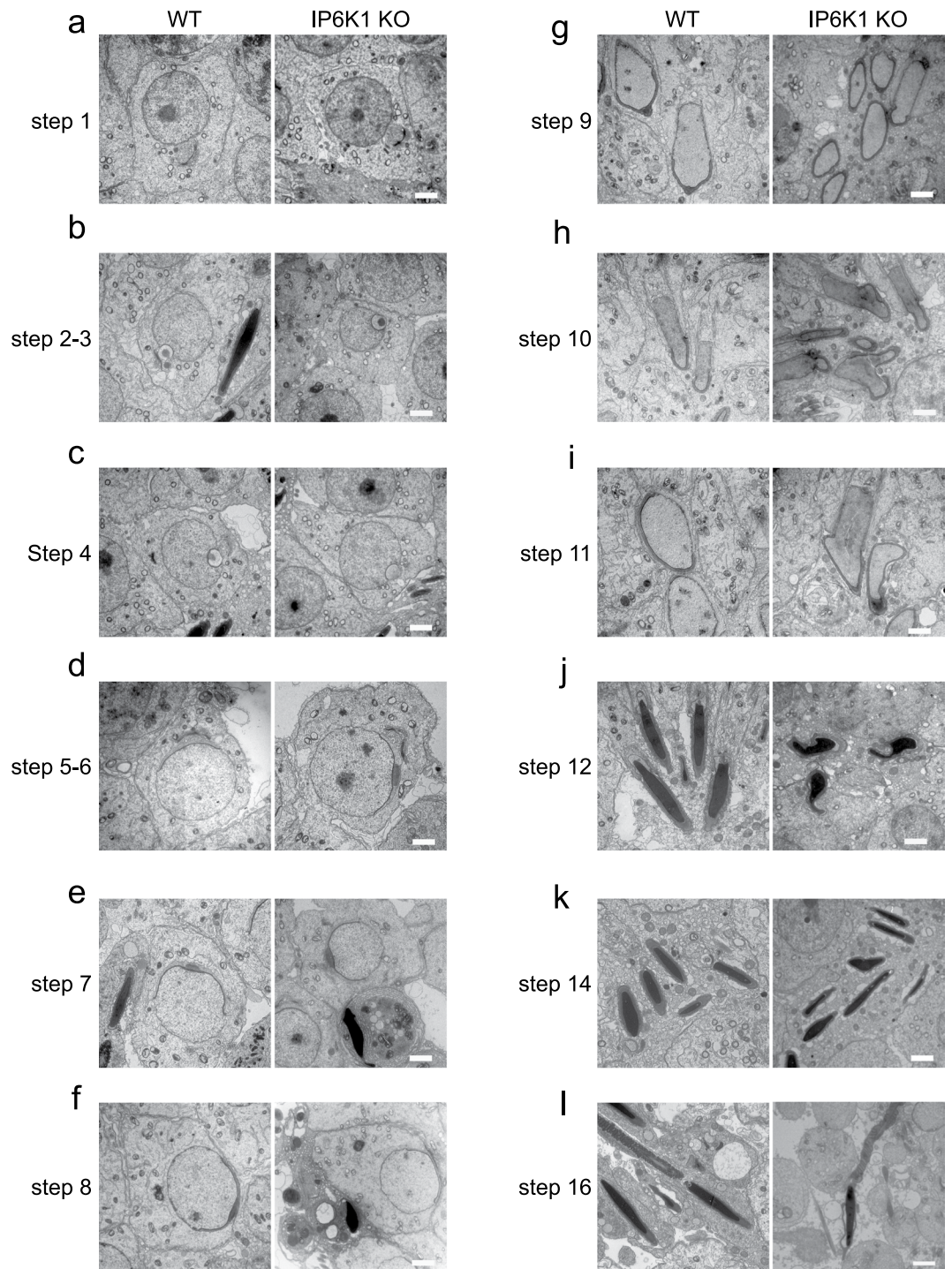


Figure 5. IP6K1 deletion caused disorientation and malformation of elongating/elongated spermatids. (a–l) Electron microscopy showed steps 1–16 spermatids from wild type and *IP6K1* KO mice. (a,b,c,d,e,f) Steps 1 to 8 round spermatids of *IP6K1* KO mice displayed relatively normal morphology. (g,h,i,j,k,l) Steps 9 to 16 elongating/elongated spermatids in *IP6K1* KO mice were disoriented and malformed. Scale bar 2 μ m.

Germ cells and Sertoli cells interact both physiologically and structurally, processes that are fundamental to male fertility^{23,34}. The apical ES is a dynamic structure, which normally organizes and orients the spermatids within the seminiferous epithelium. Fragmentation or malformation of the apical ES is associated with infertility^{22,35,36}. The apical ES comprises multiple cytoskeleton proteins, adaptor proteins and signaling proteins²². One of the most typical features of the apical ES is the array of actin filament bundles that lie perpendicular to the Sertoli cell plasma membrane and are sandwiched between the cisternae of the endoplasmic reticulum and the Sertoli cell plasma membrane^{37,38}. Emerging evidence has shown that junctional dynamics of the apical ES are supported by F-actin and the microtubule based cytoskeleton²⁵. In *IP6K1* KO mice, the apical ES were not well

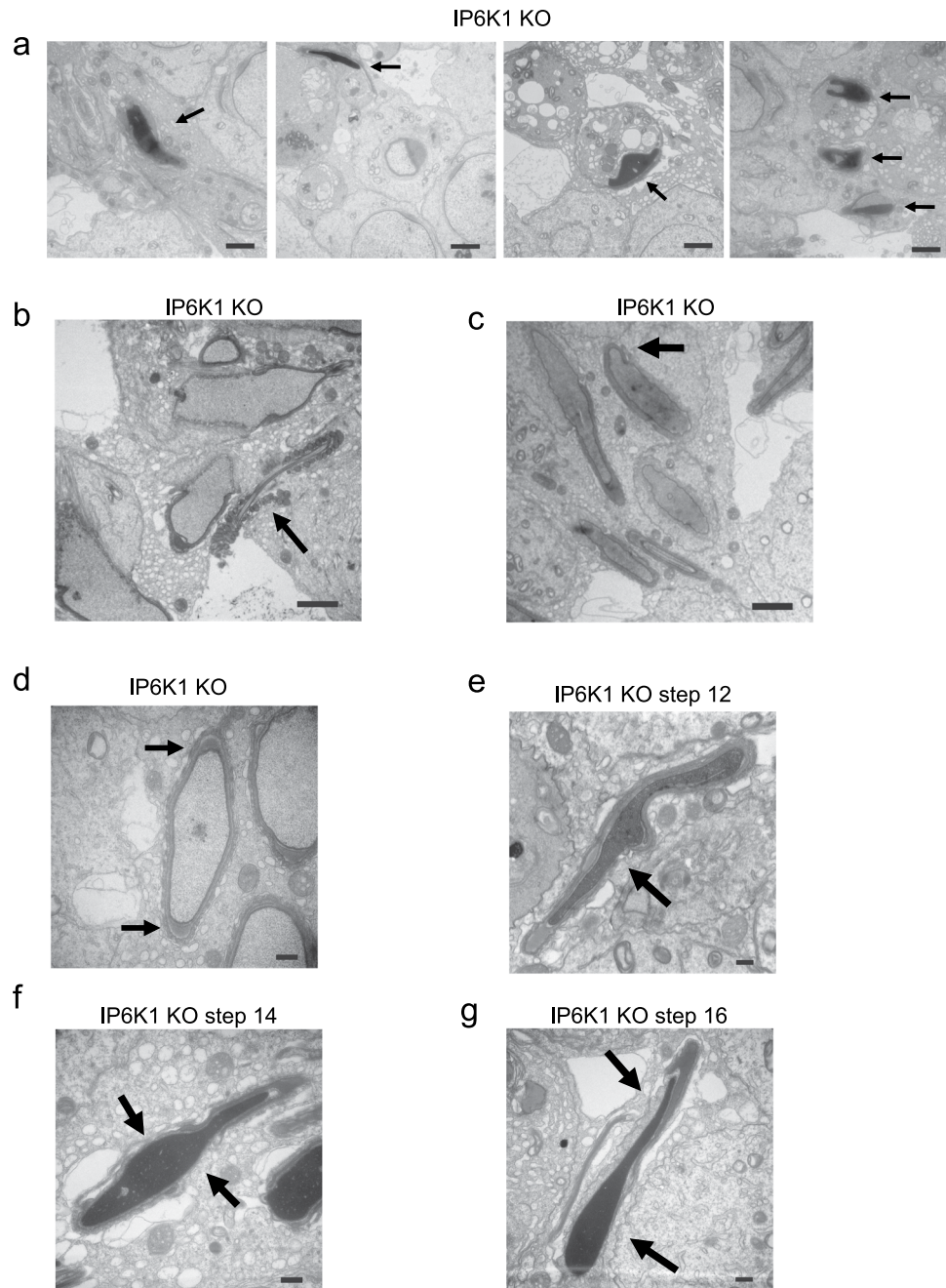


Figure 6. IP6K1 deletion disrupted spermatid cell polarity and caused degeneration of acrosomes. (a–g) Evaluation of spermatids by electron microscopy. (a) Sperm cells were engulfed (arrows) by Sertoli cells in stage VII and stage VIII seminiferous tubules of *IP6K1* KOs. Scale bar 2 μ m. (b) Severed sperm tails (arrow) showed in stage IX seminiferous tubules. Scale bar 2 μ m. (c) Disorientation of elongating spermatids (arrow) in *IP6K1* KOs. Scale bar 2 μ m. (d) Spermatids lost cell polarity in *IP6K1* KOs. Picture shows spermatid with double acrosome granules (arrow). Scale bar 2 μ m. (e) Disconnected acrosome (arrow) was evident in step 12 spermatids of *IP6K1* KOs. Scale bar 500 nm. (f) The integrity of acrosomes was disrupted (arrows) in step 14 spermatids of *IP6K1* KOs. Scale bar 500 nm. (g) The step 16 spermatids from *IP6K1* KOs lost a major part of acrosomes (arrows). Scale bar 500 nm.

formed or maintained, the actin bundle of the apical ES was collapsed in later stages of spermatid development. IP6K1's actions often are mediated by binding with other proteins^{5,7,39–41}. We have shown that IP6K1 interacts with α -actinin⁵, which regulates junctions of Sertoli cells and germ cells as well as maintaining the apical ES and spermiation⁴². These interactions with α -actinin may mediate the disrupted apical ES and spermiation in the *IP6K1* mutants. It is also possible that IP6K1 binds with junctional proteins that affect the Sertoli-germ cell interactions.

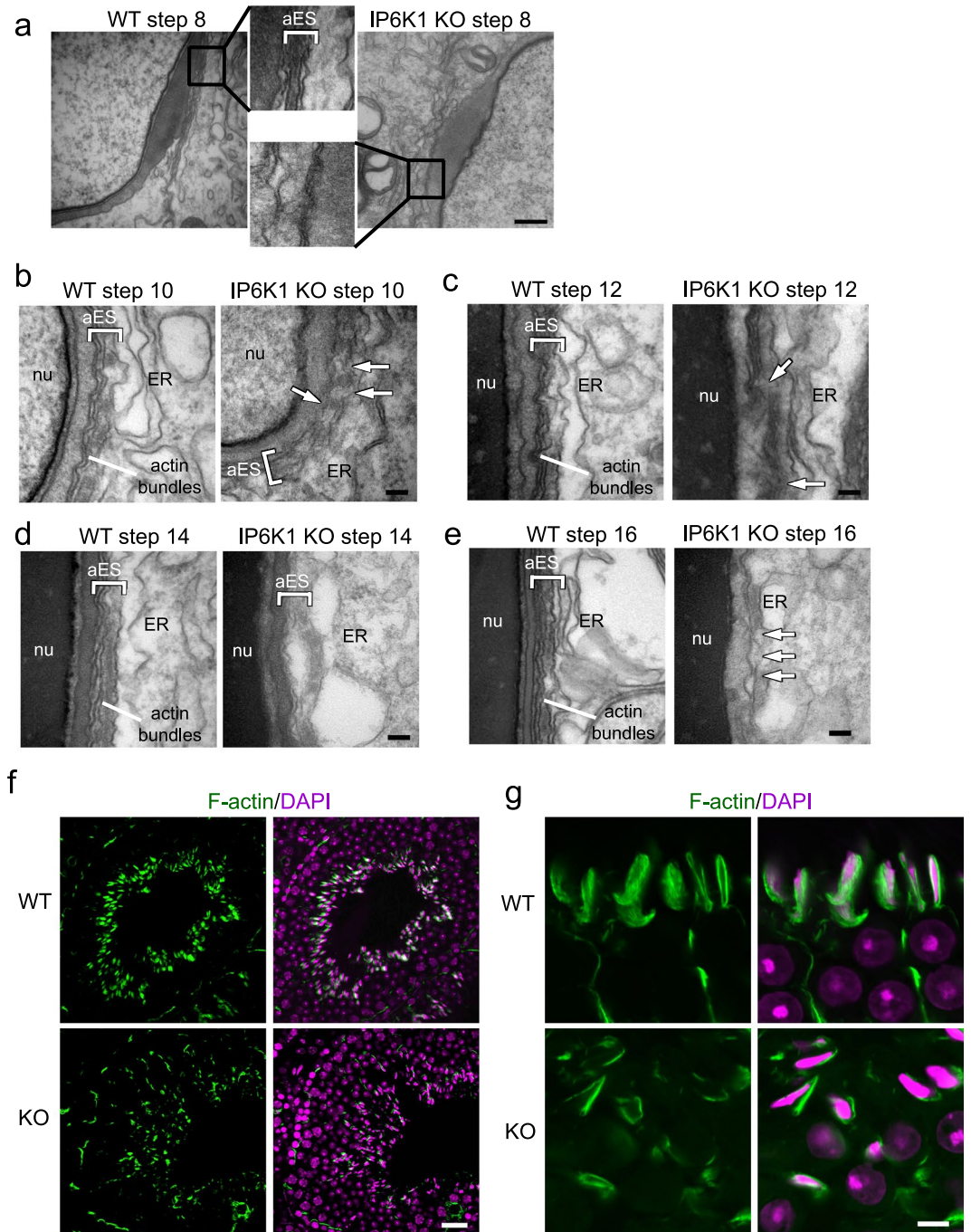


Figure 7. IP6K1 deletion disrupted apical ectoplasmic specialization. (a–e) Evaluation of spermatids by electron microscopy. (a) No characteristic apical ectoplasmic specialization (aES) was observed in step 8 spermatids of *IP6K1* KO (inset). Scale bar 500 nm. (b) The aES was not well formed in step 10 spermatids of *IP6K1* KO (arrows). ER: endoplasmic reticulum; nu: nucleus. Scale bar 100 nm. (c) Disorganized aES was seen in step 12 spermatids of *IP6K1* KO (arrows). ER: endoplasmic reticulum; nu: nucleus. Scale bar 100 nm. (d) Apical ES was collapsing in step 14 spermatids of *IP6K1* KO. ER: endoplasmic reticulum; nu: nucleus. Scale bar 100 nm. (e) Apical ES collapsed in step 16 spermatids of *IP6K1* KO (arrows). ER: endoplasmic reticulum; nu: nucleus. Scale bar 100 nm. (f and g) The actin surrounding spermatids were decreased in *IP6K1* KO. Staining of F-actin by phalloidin on seminiferous tubules. Scale bar 20 μm in (f); scale bar 5 μm in (g).

Apical ES is required for the orientation of spermatids in the seminiferous tubules. The abnormal positioning of spermatid heads of *IP6K1* KO within the epithelium is likely due to defects in the apical ES⁴³. The apical ES also plays a role in shaping the spermatid head^{44,45}. The malformation of elongated spermatids in *IP6K1* KO might be the result of defective apical ES and apical TBCs. Thus, the observed aberrations in *IP6K1* KO, such as dislodged round spermatids and malformation of elongating/elongated spermatids, might reflect defective interactions between spermatids and Sertoli cells. On the other hand, the acrosomal and nuclear shape changes

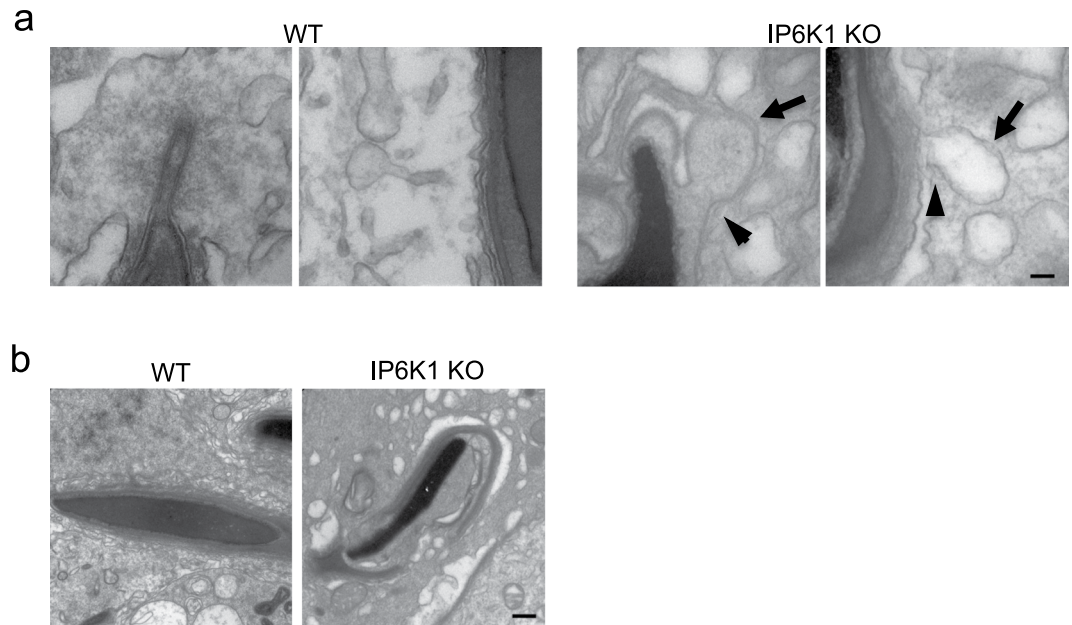


Figure 8. IP6K1 deletion disrupted spermatid-Sertoli cell interactions. **(a)** Electron microscopy showed structures of tubulobulbar complexes of WT and *IP6K1* KOs. The bulbs were enlarged (arrows) and the tubular regions were absent (arrowheads) in the *IP6K1* KOs. Scale bar 100 nm. **(b)** Electron microscopy showed step 16 spermatids from WT and *IP6K1* KO stage VII seminiferous tubules. The KO spermatids showed excess residual cytoplasm and degenerated acrosomes. Scale bar 500 nm.

in *IP6K1* KOs may also derive from deficits of the Golgi complex. Acrosomal formation requires active trafficking from the Golgi apparatus⁴⁶. IP6K1 regulates dynein-dependent trafficking pathways, and cells lacking IP6K1 display defects in Golgi maintenance⁴⁷.

Apical TBCs develop at spermatogenic stage VII, and reflect interactions between maturing spermatids and Sertoli cells. Components of apical TBCs include actin filaments, actin binding proteins, adhesion molecules and endocytic proteins²⁹. Apical TBCs remove cytoplasm from spermatids and eliminate adhesion junctions between spermatids and Sertoli cells^{26,27,32}. Defective apical TBCs fail to remove spermatid-Sertoli cell adhesions, which leads to spermiation failure^{30–32,48}. In *IP6K1* KO mice the apical TBCs were malformed with absence of proximal tubules and swelling bulbs, which may account for spermiation failure.

In *IP6K1* KOs, the interactions between spermatids and Sertoli cells were not well formed and prematurely collapsed. Deletion of IP6K1 elicited malformation of elongating/elongated spermatids. This degeneration would also eventually lead to engulfment of the spermatids by the Sertoli cells, and thereby contribute to spermiation failure^{18,19}.

IP6K1 regulates endocytic trafficking⁴⁹. Disruption of endocytosis in *EHD4* KO mice results in male infertility similar to that of *IP6K1* KO mice⁵⁰. Accordingly, the deficits of male germ cell development in *IP6K1* KOs may reflect defects of protein trafficking in membranes of the apical ES and apical TBCs.

5-IP7 affects cell-cell adhesion and adhesion-dependent signaling^{3,6}. It is uncertain whether the male infertility in *IP6K1* KOs is dependent on 5-IP7 or IP8, both products of IP6K1. The IP6K inhibitor TNP does not induce infertility in mice, which may reflect its inability to penetrate the blood-testis barrier⁵¹.

In this study, we isolated motile sperm cells after euthanizing mice with CO₂. This may not be an optimal way to obtain sperm for motility assessment, as CO₂ inhibits sperm motility⁵². Nonetheless, the deficits of *IP6K1* KO sperm cells were so striking that they are unlikely to derive primarily from CO₂ treatment.

Non-obstructive azoospermia is a common form of male infertility. Specific molecular mechanisms underlying the majority of these cases have been elusive. Our present findings, as well as the observations of Bhandari and colleagues¹¹ indicate that loss of IP6K1 affects multiple steps of sperm development. Thus IP6K1 may be a marker for male infertility with prognostic value.

Materials and Methods

Antibodies. IP6K1 (HPA040825), IP6K2 (HPA007532) and IP6K3 (SAB4500277) antibodies were from Sigma-Aldrich. Alexa Fluor™ 488 Phalloidin (A12379) was from Thermo Fisher Scientific. GATA-4 (sc-25310) and calretinin (sc-365956) antibodies were from Santa Cruz Biotechnology. Acetyl- α -Tubulin antibody (5335) was from Cell Signaling Technology.

Animals. *IP6K1*, *IP6K2* and *IP6K3* KO mice (C57BL/6) were generated by heterozygous breeding^{2,10}. The wild-type and *IP6K1* KO mice were littermates. *IP6K2/IP6K3* double knockout mice were generated by breeding *IP6K2* KOs with *IP6K3* KOs. Animal breeding and procedures were conducted in strict accordance with the NIH Guide for Care and Use of Laboratory Animals and were approved by the Johns Hopkins University Committee

on Animal Care. Mice at 10 weeks old were utilized in experiments. The investigation conformed to the Guide for the Care and Use of Laboratory Animals published by the US National Institutes of Health.

Mice sexual behavior. Male mouse sexual behavior was evaluated by examining the female's face and anogenital region. For analysis of fertility after normal mating, male mice were housed with females for 3 months. Vaginal plugs, pregnancies, and pups were recorded. Copulatory ability was determined by the appearance of vaginal plugs.

Isolation of motile sperm cells and spermatids. Male mice were euthanized by CO₂. Motile sperm cells were obtained by gently squeezing the excised epididymides; cells were collected in Krebs–Ringer solution. For collecting spermatids from testes, the testes were minced and forcefully mixed; the dislodged spermatids were collected in Krebs–Ringer solution.

Immunofluorescence staining. Wild-type and *IP6K1* KO mice were euthanized, then perfused and fixed with 4% (wt/vol) paraformaldehyde. The sections were cut 30 μm thick. The slides were blocked with 10% goat serum for 10 min, then incubated with primary antibodies (1:100 dilution) at 4 °C overnight. The fluorescence labeled secondary antibody (1:500 dilution) was incubated for 1 h at room temperature. Nuclei were counterstained with DAPI. Slices were mounted with ProLong Gold Antifade Mountant. Pictures were taken with a confocal microscope (Zeiss LSM 700, NIH Grant# S10 OD016374).

Hematoxylin and eosin staining. Wild-type and *IP6K1* KO mice were euthanized, then perfused and fixed with 4% (wt/vol) paraformaldehyde. Testes and epididymides were excised and embedded in paraffin. Sections were cut 5 μm thick and stained with hematoxylin and eosin following standard procedures.

Blood FSH, LH and testosterone. Blood samples from wild type and *IP6K1* KO mice were collected. The plasma concentrations of FSH and LH were determined by using a mouse FSH ELISA kit (Neobiolab) and a mouse LH ELISA kit (Neobiolab). The plasma concentrations of testosterone were determined by using a testosterone ELISA kit (Enzo Life Sciences).

Transmission electron microscopy and Toluidine blue staining. Wild-type and *IP6K1* KO mice were euthanized, then perfused and fixed with buffer containing 2% (wt/vol) glutaraldehyde, 2% (wt/vol) paraformaldehyde, 100 mM sodium cacodylate and 3 mM MgCl₂, pH 7.4. Testes were excised and post-fixed in 1.5% potassium ferrocyanide reduced 2% osmium tetroxide in 100 mM sodium cacodylate with 3 mM MgCl₂ for 2 h on ice in the dark. After a brief rinse in 100 mM maleate buffer containing 3% sucrose, samples were placed in 2% uranyl acetate in maleate/sucrose for 1 h at 4 °C with slow rocking in the dark. Samples were then dehydrated through a graded series of ethanol, transferred through propylene oxide and were embedded in Eponate 12 Resin and cured at 60 °C for two days.

For transmission electron microscopy, sections were cut 80 nm thick and stained with uranyl acetate followed by lead citrate. Grids were viewed on a Hitachi 7600 TEM operating at 80 kV and digital images captured with an XR50 (5 megapixel) CCD camera.

For Toluidine blue staining, sections were cut 0.5 μm thick and stained with 1% toluidine blue and 1% sodium borate for 1 min.

Statistical analysis. Quantitative data are expressed as means ± SEM. Data were analyzed by unpaired Student's t-test. $P < 0.05$ was considered statistically significant. For non-quantitative data, results were representative of at least 3 independent experiments.

Data Availability. All data generated or analysed during this study are included in this published article (and its Supplementary Information files).

References

- Bhandari, R., Juluri, K. R., Resnick, A. C. & Snyder, S. H. Gene deletion of inositol hexakisphosphate kinase 1 reveals inositol pyrophosphate regulation of insulin secretion, growth, and spermiogenesis. *Proc Natl Acad Sci USA* **105**, 2349–2353, <https://doi.org/10.1073/pnas.0712227105> (2008).
- Fu, C. *et al.* Inositol Hexakisphosphate Kinase-3 Regulates the Morphology and Synapse Formation of Cerebellar Purkinje Cells via Spectrin/Adducin. *J Neurosci* **35**, 11056–11067, <https://doi.org/10.1523/JNEUROSCI.1069-15.201535/31/11056> (2015).
- Rao, E. *et al.* Inositol pyrophosphates promote tumor growth and metastasis by antagonizing liver kinase B1. *Proc Natl Acad Sci USA* **112**, 1773–1778, <https://doi.org/10.1073/pnas.1424642112> (2015).
- Illies, C. *et al.* Requirement of inositol pyrophosphates for full exocytotic capacity in pancreatic beta cells. *Science* **318**, 1299–1302, [1146824](https://doi.org/10.1126/science.1146824) (2007).
- Fu, C. *et al.* Neuronal migration is mediated by inositol hexakisphosphate kinase 1 via alpha-actinin and focal adhesion kinase. *Proc Natl Acad Sci USA* **114**, 2036–2041, <https://doi.org/10.1073/pnas.1700165114> (2017).
- Jadav, R. S. *et al.* Deletion of inositol hexakisphosphate kinase 1 (IP6K1) reduces cell migration and invasion, conferring protection from aerodigestive tract carcinoma in mice. *Cell Signal* **28**, 1124–1136, [https://doi.org/10.1016/j.cellsig.2016.04.011S0898-6568\(16\)30097-3](https://doi.org/10.1016/j.cellsig.2016.04.011S0898-6568(16)30097-3) (2016).
- Burton, A., Azevedo, C., Andreassi, C., Riccio, A. & Saiardi, A. Inositol pyrophosphates regulate JMJD2C-dependent histone demethylation. *Proc Natl Acad Sci USA* **110**, 18970–18975, <https://doi.org/10.1073/pnas.1309699110> (2013).
- Zhu, Q. *et al.* Adipocyte-specific deletion of Ip6k1 reduces diet-induced obesity by enhancing AMPK-mediated thermogenesis. *J Clin Invest* **126**, 4273–4288, [10.1172/JCI85510](https://doi.org/10.1172/JCI85510) (2016).
- Boregowda, S. V. *et al.* IP6K1 Reduces Mesenchymal Stem/Stromal Cell Fitness and Potentiates High Fat Diet-Induced Skeletal Involution. *Stem Cells* **35**, 1973–1983, <https://doi.org/10.1002/stem.2645> (2017).
- Chakraborty, A. *et al.* Inositol pyrophosphates inhibit Akt signaling, thereby regulating insulin sensitivity and weight gain. *Cell* **143**, 897–910, [https://doi.org/10.1016/j.cell.2010.11.032S0092-8674\(10\)01349-8](https://doi.org/10.1016/j.cell.2010.11.032S0092-8674(10)01349-8) (2010).

11. Malla, A. B. & Bhandari, R. IP6K1 is essential for chromatoid body formation and temporal regulation of Tnp2 and Prm2 expression in mouse spermatids. *J Cell Sci* **130**, 2854–2866, <https://doi.org/10.1242/jcs.204966> (2017).
12. Cheng, C. Y., Wong, E. W., Yan, H. H. & Mruk, D. D. Regulation of spermatogenesis in the microenvironment of the seminiferous epithelium: new insights and advances. *Mol Cell Endocrinol* **315**, 49–56, <https://doi.org/10.1016/j.mce.2009.08.004> (2010).
13. Griswold, M. D. The central role of Sertoli cells in spermatogenesis. *Semin Cell Dev Biol* **9**, 411–416, S1084-9521(98)90203-8 10.1006/scdb.1998.0203 (1998).
14. Alves, M. G. *et al.* Hormonal control of Sertoli cell metabolism regulates spermatogenesis. *Cell Mol Life Sci* **70**, 777–793, <https://doi.org/10.1007/s00018-012-1079-1> (2013).
15. Shi, J. F. *et al.* Characterization of cholesterol metabolism in Sertoli cells and spermatogenesis (Review). *Mol Med Rep* **17**, 705–713, <https://doi.org/10.3892/mmr.2017.8000> (2018).
16. Franca, L. R., Hess, R. A., Dufour, J. M., Hofmann, M. C. & Griswold, M. D. The Sertoli cell: one hundred fifty years of beauty and plasticity. *Andrology* **4**, 189–212, <https://doi.org/10.1111/andr.12165> (2016).
17. Kaur, G., Thompson, L. A. & Dufour, J. M. Sertoli cells—immunological sentinels of spermatogenesis. *Semin Cell Dev Biol* **30**, 36–44, <https://doi.org/10.1016/j.semcdb.2014.02.011> S1084-9521(14)00023-8 (2014).
18. Russell, L. D. & Clermont, Y. Degeneration of germ cells in normal, hypophysectomized and hormone treated hypophysectomized rats. *Anat Rec* **187**, 347–366, <https://doi.org/10.1002/ar.1091870307> (1977).
19. Chemes, H. The phagocytic function of Sertoli cells: a morphological, biochemical, and endocrinological study of lysosomes and acid phosphatase localization in the rat testis. *Endocrinology* **119**, 1673–1681, <https://doi.org/10.1210/endo-119-4-1673> (1986).
20. Oakberg, E. F. Duration of spermatogenesis in the mouse and timing of stages of the cycle of the seminiferous epithelium. *Am J Anat* **99**, 507–516, <https://doi.org/10.1002/aja.1000990307> (1956).
21. Kopera, I. A., Bilinska, B., Cheng, C. Y. & Mruk, D. D. Sertoli-germ cell junctions in the testis: a review of recent data. *Philos Trans R Soc Lond B Biol Sci* **365**, 1593–1605, <https://doi.org/10.1098/rstb.2009.0251> 365/1546/1593 (2010).
22. Lee, N. P. & Cheng, C. Y. Ectoplasmic specialization, a testis-specific cell-cell actin-based adherens junction type: is this a potential target for male contraceptive development? *Hum Reprod Update* **10**, 349–369, <https://doi.org/10.1093/humupd/dmh026> (2004).
23. Syed, V. & Hecht, N. B. Disruption of germ cell-Sertoli cell interactions leads to spermatogenic defects. *Mol Cell Endocrinol* **186**, 155–157, doi:S0303720701006566 (2002).
24. Glikli, G., Ebnet, K., Aurrand-Lions, M., Imhof, B. A. & Adams, R. H. Spermatid differentiation requires the assembly of a cell polarity complex downstream of junctional adhesion molecule-C. *Nature* **431**, 320–324, <https://doi.org/10.1038/nature02877> (2004).
25. Wen, Q. *et al.* Transport of germ cells across the seminiferous epithelium during spermatogenesis—the involvement of both actin- and microtubule-based cytoskeletons. *Tissue Barriers* **4**, e1265042, <https://doi.org/10.1080/21688370.2016.1265042> (2016).
26. Vogl, A. W., Young, J. S. & Du, M. New insights into roles of tubulobulbar complexes in sperm release and turnover of blood-testis barrier. *Int Rev Cell Mol Biol* **303**, 319–355, <https://doi.org/10.1016/B978-0-12-407697-6.00008-8> (2013).
27. Russell, L. D. Spermatid-Sertoli tubulobulbar complexes as devices for elimination of cytoplasm from the head region late spermatids of the rat. *Anat Rec* **194**, 233–246, <https://doi.org/10.1002/ar.1091940205> (1979).
28. Guttman, J. A., Takai, Y. & Vogl, A. W. Evidence that tubulobulbar complexes in the seminiferous epithelium are involved with internalization of adhesion junctions. *Biol Reprod* **71**, 548–559, <https://doi.org/10.1095/biolreprod.104.028803> (2004).
29. Upadhyay, R. D., Kumar, A. V., Ganeshan, M. & Balasinar, N. H. Tubulobulbar complex: cytoskeletal remodeling to release spermatozoa. *Reprod Biol Endocrinol* **10**, 27, <https://doi.org/10.1186/1477-7827-10-27> (2012).
30. Kusumi, N. *et al.* Implication of amphiphysin 1 and dynamin 2 in tubulobulbar complex formation and spermatid release. *Cell Struct Funct* **32**, 101–113, JSTJSTAGE/csf/07024 (2007).
31. D'Souza, R. *et al.* Disruption of tubulobulbar complex by high intratesticular estrogens leading to failed spermiation. *Endocrinology* **150**, 1861–1869, <https://doi.org/10.1210/en.2008-1232> (2009).
32. Young, J. S., De Asis, M., Guttman, J. & Vogl, A. W. Cortactin depletion results in short tubulobulbar complexes and spermiation failure in rat testes. *Biol Open* **1**, 1069–1077, <https://doi.org/10.1242/bio.20122519> (2012).
33. Lie, P. P., Chan, A. Y., Mruk, D. D., Lee, W. M. & Cheng, C. Y. Restricted Arp3 expression in the testis prevents blood-testis barrier disruption during junction restructuring at spermatogenesis. *Proc Natl Acad Sci USA* **107**, 11411–11416, <https://doi.org/10.1073/pnas.1001823107> (2010).
34. Johnston, D. S. *et al.* Stage-specific gene expression is a fundamental characteristic of rat spermatogenic cells and Sertoli cells. *Proc Natl Acad Sci USA* **105**, 8315–8320, <https://doi.org/10.1073/pnas.0709854105> (2008).
35. Cai, H. *et al.* Scrotal heat stress causes a transient alteration in tight junctions and induction of TGF-beta expression. *Int J Androl* **34**, 352–362, <https://doi.org/10.1111/j.1365-2605.2010.01089.x> IJA1089 (2011).
36. Lyon, K. *et al.* Ca²⁺ signaling machinery is present at intercellular junctions and structures associated with junction turnover in rat Sertoli cells. *Biol Reprod*. <https://doi.org/10.1093/biolre/iox0423806625> (2017).
37. Cheng, C. Y. & Mruk, D. D. A local autocrine axis in the testes that regulates spermatogenesis. *Nat Rev Endocrinol* **6**, 380–395, <https://doi.org/10.1038/nrendo.2010.71> (2010).
38. Vogl, A. W., Vaid, K. S. & Guttman, J. A. The Sertoli cell cytoskeleton. *Adv Exp Med Biol* **636**, 186–211, https://doi.org/10.1007/978-0-387-09597-4_11 (2008).
39. Chakraborty, A., Latapy, C., Xu, J., Snyder, S. H. & Beaulieu, J. M. Inositol hexakisphosphate kinase-1 regulates behavioral responses via GSK3 signaling pathways. *Mol Psychiatry* **19**, 284–293, <https://doi.org/10.1038/mp.2013.21> (2014).
40. Rao, F. *et al.* Inositol hexakisphosphate kinase-1 mediates assembly/disassembly of the CRL4-signalosome complex to regulate DNA repair and cell death. *Proc Natl Acad Sci USA* **111**, 16005–16010, <https://doi.org/10.1073/pnas.1417900111> (2014).
41. Ghoshal, S., Tyagi, R., Zhu, Q. & Chakraborty, A. Inositol hexakisphosphate kinase-1 interacts with perilipin1 to modulate lipolysis. *Int J Biochem Cell Biol* **78**, 149–155, S1357-2725(16)30158-3 10.1016/j.biocel.2016.06.018 (2016).
42. Zhang, J. *et al.* Regulation of Sertoli-germ cell adherens junction dynamics via changes in protein-protein interactions of the N-cadherin-beta-catenin protein complex which are possibly mediated by c-Src and myotubularin-related protein 2: an *in vivo* study using an androgen suppression model. *Endocrinology* **146**, 1268–1284, en.2004-1194 10.1210/en.2004-1194 (2005).
43. Yan, H. H., Mruk, D. D., Lee, W. M. & Cheng, C. Y. Ectoplasmic specialization: a friend or a foe of spermatogenesis? *Bioessays* **29**, 36–48, <https://doi.org/10.1002/bies.20513> (2007).
44. Cheng, C. Y. & Mruk, D. D. Actin binding proteins and spermiogenesis: Some unexpected findings. *Spermatogenesis* **1**, 99–104, <https://doi.org/10.4161/spmg.1.2.169132156-5554-1-2-4> (2011).
45. Kierszenbaum, A. L. & Tres, L. L. The acrosome-acroplaxome-manchette complex and the shaping of the spermatid head. *Arch Histol Cytol* **67**, 271–284 (2004).
46. Berruti, G. & Paiardi, C. Acrosome biogenesis: Revisiting old questions to yield new insights. *Spermatogenesis* **1**, 95–98, <https://doi.org/10.4161/spmg.1.2.168202156-5554-1-2-3> (2011).
47. Chanduri, M. *et al.* Inositol hexakisphosphate kinase 1 (IP6K1) activity is required for cytoplasmic dynein-driven transport. *Biochem J* **473**, 3031–3047, <https://doi.org/10.1042/BCJ20160610> (2016).
48. O'Donnell, L. Mechanisms of spermiogenesis and spermiation and how they are disturbed. *Spermatogenesis* **4**, e979623, <https://doi.org/10.4161/21565562.2014.979623> (2014).

49. Saiardi, A., Sciambi, C., McCaffery, J. M., Wendland, B. & Snyder, S. H. Inositol pyrophosphates regulate endocytic trafficking. *Proc Natl Acad Sci USA* **99**, 14206–14211, <https://doi.org/10.1073/pnas.212527899> (2002).
50. George, M. *et al.* Ehd4 is required to attain normal prepubertal testis size but dispensable for fertility in male mice. *Genesis* **48**, 328–342, <https://doi.org/10.1002/dvg.20620> (2010).
51. Ghoshal, S. *et al.* TNP [N2-(m-Trifluorobenzyl), N6-(p-nitrobenzyl)purine] ameliorates diet induced obesity and insulin resistance via inhibition of the IP6K1 pathway. *Mol Metab* **5**, 903–917, [https://doi.org/10.1016/j.molmet.2016.08.008S2212-8778\(16\)30125-9](https://doi.org/10.1016/j.molmet.2016.08.008S2212-8778(16)30125-9) (2016).
52. Ingermann, R. L., Holcomb, M., Robinson, M. L. & Cloud, J. G. Carbon dioxide and pH affect sperm motility of white sturgeon (*Acipenser transmontanus*). *J Exp Biol* **205**, 2885–2890 (2002).

Acknowledgements

We thank Dr. A. Wayne Vogl at University of British Columbia, Dr. Rex A Hess at University of Illinois, Dr. Barry Zirkin and Dr. Haolin Chen at Johns Hopkins Bloomberg School of Public Health for advices. We thank Michael Delannoy and Barbara Smith at the Johns Hopkins SOM Microscope Facility for technical support of the transmission electron microscopy. We also thank Pamela Wright for editing the manuscript. This work was supported by USPHS grants MH18501 and DA000266.

Author Contributions

C.F., W.W.W. and S.H.S. designed the experiments. C.F., T.R., A.C.C., W.C., I.A.B. and L.K.A. performed experiments. C.F., T.R., W.W.W. and S.H.S. analyzed data and wrote the manuscript.

Additional Information

Supplementary information accompanies this paper at <https://doi.org/10.1038/s41598-018-25468-8>.

Competing Interests: The authors declare no competing interests.

Publisher's note: Springer Nature remains neutral with regard to jurisdictional claims in published maps and institutional affiliations.



Open Access This article is licensed under a Creative Commons Attribution 4.0 International License, which permits use, sharing, adaptation, distribution and reproduction in any medium or format, as long as you give appropriate credit to the original author(s) and the source, provide a link to the Creative Commons license, and indicate if changes were made. The images or other third party material in this article are included in the article's Creative Commons license, unless indicated otherwise in a credit line to the material. If material is not included in the article's Creative Commons license and your intended use is not permitted by statutory regulation or exceeds the permitted use, you will need to obtain permission directly from the copyright holder. To view a copy of this license, visit <http://creativecommons.org/licenses/by/4.0/>.

© The Author(s) 2018